Kinetic Analysis of Sequence-Specific Recognition of ssDNA by an Autoantibody†

Jennifer A. Beckingham,‡ Joanne Cleary,‡ Melissa Bobeck,‡ and Gary D. Glick*,‡,§

Departments of Chemistry and Biological Chemistry, University of Michigan, Ann Arbor, Michigan 48109-1055

Received November 15, 2002

ABSTRACT: 11F8 is a pathogenic monoclonal anti-ssDNA autoantibody isolated from a lupus prone mouse. Previous studies established that 11F8 is sequence-specific and identified the thermodynamic and kinetic basis for the specific recognition of ssDNA, and binding site mutations of a single-chain construct reveal that ^{Y32}LCDR1, ^{R31}HCDR1, ^{W33}HCDR1, ^{R98}HCDR3, ^{L97}HCDR3, and ^{Y100}HCDR3 are responsible for approximately 80% of the binding free energy. Here we evaluate the role of these residues along with a group of basic residues (K62, K64, R24, K52) within the context of the binding mechanism. Binding of 11F8 takes place in two steps. In the first step, the overall positive charge of the antigen binding site attracts the negatively charged DNA to form an encounter complex that is stabilized by two salt bridges and a hydrogen bond. The second step is a slow process in which minor conformational changes occur. During this step, aromatic side chains become desolvated, presumably through stacking interactions involving two thymine bases within the DNA recognition epitope. Although the stability of the complex arises primarily from interactions formed in the second step, sequence specificity results from interactions with residues involved in both steps. These studies also show that the way in which 11F8 achieves high affinity sequence-specific binding is more closely related to RNA binding proteins than those that bind DNA and point to strategies for disrupting DNA binding that could prove to be therapeutically useful.

Antibodies that bind nucleic acids provide a unique framework to study protein·nucleic acid interactions (*1*). Although canonical B-form DNA is not generally immunogenic, it is possible to experimentally induce antibodies to B-DNA (*2*) along with other forms of nucleic acids such as hairpin loops (*3*). Antibodies that bind DNA (anti-DNA) also arise spontaneously as a result of several different rheumatic diseases and are the most prominent serological hallmark of the autoimmune disorder systemic lupus erythematosus (SLE) (*4*, *5*). In addition to being diagnostic, a subset of anti-DNA trigger an inflammatory response (known as lupus nephritis or glomerulonephritis) that results in renal damage which can be fatal (*6*, *7*).

In previous studies we generated a panel of anti-ssDNA monoclonal autoantibodies (mAb) from an autoimmune MRL/*lpr* mouse (*8*). One mAb from this panel, 11F8, binds to DNA adherent to the glomerular basement membrane (*9*), which, for some anti-DNA-like 11F8, is the first critical step in the series of events leading to lupus nephritis. Through binding-site selection experiments, footprinting, and affinity measurements, we have provided evidence that 11F8 is sequence-specific (*10*). Sequence-specific recognition by 11F8 is achieved when functional groups on the single-stranded epitope-TTC− of its high affinity consensus sequence (**1**) are presented within a well-defined secondary structure (Figure 1). Although **1** was identified using binding site selection experiments, its sequence and structure are closely related to DNA antigens present in human anti-DNA·

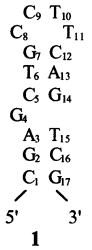

1

FIGURE 1: High-affinity 11F8 consensus sequence, **1**, is a 19-mer that adopts a stem-loop ("hairpin") conformation with a bulge base in position 4. Residues 10−12 provide critical sequence-dependent recognition contacts, whereas the bases in the stem duplex, including the bulge, serve only to preorganize the recognition elements (*12*). This sequence is a truncated analogue of the 55-mer identified through binding-site selection experiments (*10*). Although the original selection construct was designed to prevent the formation of a stable secondary structure, mutations produced during PCR amplification at multiple sites within the constant region afforded a stable secondary structure that was selected for by 11F8. Truncation removes the PCR primers used in the selection process but does not cause a decrease in affinity. The base at residue 4 was replaced with 2-aminopurine (AP) to introduce a unique fluorescent label within the DNA structure. Due to fraying at the stem-loop junction, dC_{12} possesses single-strand character, as evidenced by NMR and its reactivity to single-strand specific footprinting reagents (*10*).

DNA complexes (*11*). Binding of **1** is enthalpy-driven, opposed by entropy, and accompanied by a negative change in heat capacity (*12*). The thermodynamic driving force for sequence specificity is the release of incompletely hydrogen-bonded water molecules from the hydrophobic binding site, concomitant with the formation of two salt bridges (*12*). The interaction between 11F8 and **1** follows a two step mechanism indicative of induced fit binding. First, a bimolecular association occurs that is dominated by electrostatic forces,

† Supported by NIH Grant GM 42168.

* Corresponding author. Phone: (734) 764-4548. Fax: (734) 615-8902. E-mail gglick@umich.edu.

‡ Department of Chemistry.

§ Department of Biological Chemistry.

10.1021/bi020658k CCC: $25.00
Published on Web 03/18/2003

including the formation of two salt bridges. This step is followed by a slow conformational change, leading to the high-affinity complex observed at equilibrium. Dissociation of the complex is rate-limited by the reversal of the isomerization process (*13*).

Site-directed mutagenesis experiments using an 11F8 single-chain construct (sc11F8) designed to elucidate the role of basic and hydrophobic residues in specific, noncognate and nonspecific binding demonstrate that six amino acids residues within the complementarity determining regions (CDRs)[1] contribute to ~80% of the binding free energy (*14*). Here we describe the function of these residues in context of the binding mechanism. Our data reveal that the overall stability of the complex chiefly arises through the interactions that occur during the second binding step. However, sequence specificity is mediated through interactions that take place in both binding steps. Although 11F8 binds ssDNA, our studies reveal that this system reflects many features that are exhibited by protein·RNA complexes and may help to explain why 11F8 is pathogenic.

MATERIALS AND METHODS

Preparation of Mutant Proteins and DNA Ligands. The construction, expression, and purification of the sc11F8 has been described elsewhere (*14*). Mutants K62Q, K64Q, $R24_LQ$, $K52_LQ$, and one with all four basic residues replaced with glutamine designated Quad were constructed using Quickchange Site-Directed Mutagenesis Kit (Stratagene). The mutant proteins were expressed and purified as the wild-type protein. The DNA sequences used in binding studies were synthesized and purified as previously described (*12*). Guanidine hydrochloride denaturation experiments to determine the stability of the mutant proteins were conducted as described by Cleary and Glick (*14*).

Steady-State Fluorescence Measurements. Steady-state fluorescence measurements were made using a Spectronic AB2 fluorimeter as described by Ackroyd et al. (*12*). For monitoring tryptophan fluorescence, the excitation wavelength was set at 280 nm and emission wavelength at 336 nm. To measure the emission of the AP, the excitation wavelength was set at 310 nm and emission wavelength at 360 nm, with the slit widths set at 4 and 8 mm for the excitation and emission wavelengths, respectively. For binding isotherms, data were collected over a 10 s period allowing 30 s from each addition of DNA for equilibration to occur. No correction for the inner filter effect was necessary. Analysis of the binding isotherms has been described elsewhere (*12*).

Stopped-Flow Measurements. Stopped-flow measurements were conducted using a π*-CDF or SX·18MV stopped-flow spectrophotometer from Applied Photophysics Ltd. (Surrey, UK). The sample-handling unit was fitted with 2 mL syringes to give a mixing ratio of 1:1 v/v. The slit widths were set at 1.5 nm, and 1000 data points were collected for each measurement over a range of time periods. The excitation wavelengths were the same as used for the equilibrium experiments and the emission of the different fluorescent groups was monitored through the use of suitable cutoff filters. All measurements were made in 20 mM Tris-HCl, pH 8.0, 100 mM NaCl, 20% w/v sucrose unless otherwise stated. Each experiment was carried out at least five times, analyzed both individually and as an average by single or double exponential curve fitting algorithms using the software supplied with the instrument.

In experiments to determine the association rates for complex formation, [sc11F8] = 200 nM (all concentrations given are prior to mixing) while the DNA was maintained in at least a 10-fold excess, to approximate pseudo-first-order reaction conditions. From the plot of [DNA] versus k_{app}, the apparent second-order rate constants, k_{on}, were calculated from the slope and the dissociation of the complex, k_{off}, calculated from the *y*-intercept. The affinity of the complex was calculated from the relationship $K_d = k_{off}/k_{on}$. Dissociation experiments were carried out by mixing a preformed complex (sc11F8·**1**AP), with a 10-fold excess of **1** (1:1 v/v) unless otherwise stated. The fluorescence of the AP was monitored as the complex dissociated. The resulting reaction trace was analyzed by a single-exponential equation.

Analysis of the Temperature Dependence of the Association and Dissociation Rate Constants. The pre-equilibrium experiments were repeated over the temperature range of 5−35 ± 0.1 °C to determine the thermodynamic parameters for the second binding step. The activation energy from each step was calculated from the Arrhenius equation:

$$k = A\, e^{-E_a/RT} \quad (1)$$

where k is the rate constant and E_a is the activation energy. The slope of the plot $1/T$ versus ln k gives $-E_a/RT$. The enthalpy and entropy of activation were determined using the Eyring equation:

$$k = (k_B T\kappa/h)\cdot e^{(\Delta S^{\ddagger}/R)}\cdot e^{(-\Delta H^{\ddagger}/RT)} \quad (2)$$

where k is the rate constant, k_B is Boltzman constant, h is Planck's constant, and $\Delta H^{\ddagger}$ and $\Delta S^{\ddagger}$ are the enthalpy and entropy of activation, respectively. The plot of $1/T$ versus $\ln(k/T)$ gives a slope of $-\Delta H^{\ddagger}/RT$ and a *y*-intercept of $\ln(k_B/h) + \Delta S^{\ddagger}/R$.

RESULTS

*Binding Mechanism for the sc11F8·**1** Complex.* The binding mechanism identified for the interaction between the parent 11F8 IgG and **1** is shown in Scheme 1. Binding occurs

Scheme 1

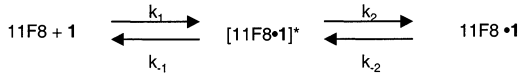

in two steps: formation of an encounter complex followed by a slow, rate-limiting step that results in the high-affinity complex observed at equilibrium (*13*). Previous studies have shown that the thermodynamic parameters associated with the interaction between sc11F8 and **1** are indistinguishable from those of 11F8 F(ab) and **1**, making sc11F8 a suitable

[1] Abbreviations: anti-DNA, anti-DNA autoantibodies; CDR, complementarity determining region; mAb, monoclonal antibodies; ssDNA, single-stranded DNA; sc11F8, 11F8 single-chain antibody fragment; SLE, systemic lupus erythematosus; ^{a}X, where a represents the amino acid and X denotes the CDR; V_x, where V donates the variable domains of the antibody and X identifies whether it is from the light (L) or heavy (H) chain; AP, 2-aminopurine.

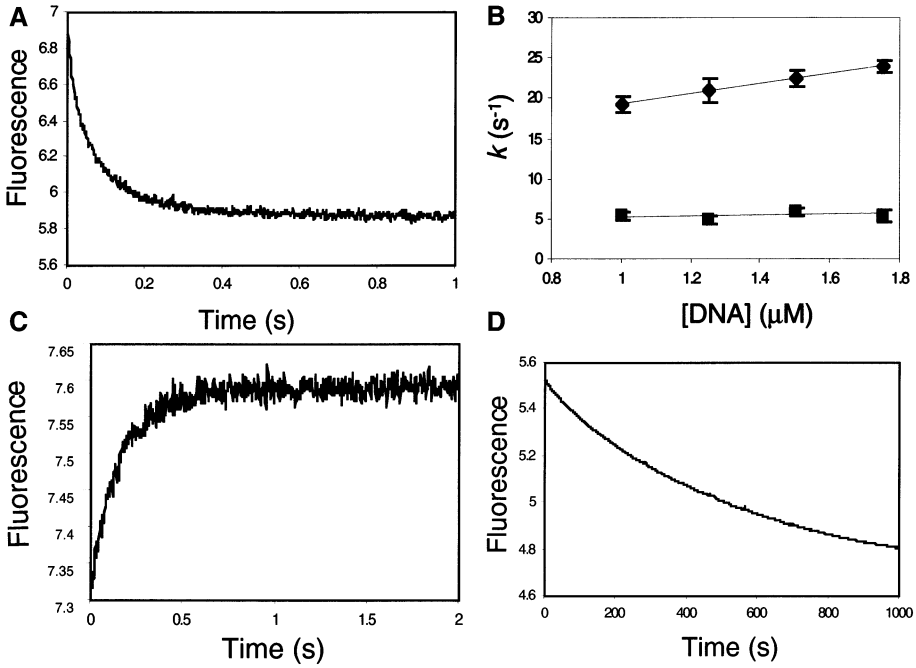

FIGURE 2: Stopped-flow fluorescence results for the interaction between sc11F8 and **1**. (A) Association trace for the interaction between **1** (2 μM) and sc11F8 (200 nM). The excitation wavelength was set at 280 nm to monitor tryptophan fluorescence. The initial fast change in fluorescence has a rate of 20.8 s^{-1}, whereas the rate of the second slow signal change is 5.8 s^{-1}. (B) Linear dependence of the initial rate (k_{app}) on [**1**] (◆). The second-order rate constant (k_1) in 20% sucrose was calculated to be 5.9 μM^{-1} s^{-1} from the slope of the plot and $k_{-1} = 13.5$ s^{-1} from the *y*-intercept. The second slower rate (■) observed was shown to be independent of [**1**] over the concentration range tested. (C) Dissociation of the sc11F8·**1**AP complex, where the preformed complex was mixed with an excess of **1** that binds rapidly to the newly dissociated sc11F8. The excitation wavelength was set at 310 nm to monitor the dissociation of sc11F8·**1**AP. (D) Association of sc11F8 (200 nM) with **1**AP (2 μM) with the excitation wavelength set at 310 nm to monitor changes in AP fluorescence. A single fluorescence change was observed with a rate (6.3 s^{-1}) comparable to the slow rate observed between the interaction of sc11F8 and **1**. This rate was also independent of [**1**AP].

Table 1: Kinetic Parameters for the Association and Dissociation of sc11F8 Measured at 20% w/v Sucrose at 5 °C

complex	k_1 (μM^{-1} s^{-1})	k_{-1} (s^{-1})	k_2 (s^{-1})	k_{-2} (s^{-1})	K_d (nM)
11F8·**1**	9.4 ± 1.1	5.7 ± 0.44	3.8 ± 0.21	0.00293 ± 0.0002	0.41 ± 0.2
sc11F8·**1**	5.93 ± 0.64	13.5 ± 1.4	6.43 ± 0.34	−	0.31 ± 0.1
sc11F8·**1**AP	−	−	6.36 ± 0.73	0.00075 ± 0.00006	0.34 ± 0.1

model for mutagenesis studies (*14*). However, to ensure that the kinetic parameters were also analogous to the parent antibody, the rates of association and dissociation of the sc11F8·**1** complex were measured.

On binding DNA, a quench in the intrinsic tryptophan fluorescence of 11F8 is observed (*8*). sc11F8 contains five tryptophan residues, ^{W33}HCDR1, which lies within the proposed binding pocket, and ^{W36}HFW2, ^{W47}HFW2, ^{W103}HFW4, and ^{W35}LFW2, all of which reside within three residues of a CDR loop (*9*, *14*, *15*). The change in emission upon DNA binding enables the kinetic parameters for complex formation to be determined by stopped-flow fluorescence techniques.

The rate of association of the complex was measured by mixing a constant concentration of sc11F8 with an excess of **1** (10−17.5-fold). Similar to 11F8 binding, the initial signal changes are too rapid to measured accurately; therefore, sucrose (20% w/v) was added to the buffers and the temperature decreased to 5 °C to increase the viscosity, thereby decreasing the apparent rate (k_{app}). The reaction curve for the association of the sc11F8 and **1** is biphasic, where an initial fast decrease accounts for <15% of the total signal change (Figure 2A), comparable to that observed with the binding of **1** by 11F8 (*13*). This initial rate is linearly dependent on [**1**], typical of a simple bimolecular association process (Figure 2B). The second-order rate constant, k_1, and dissociation rate, k_{-1}, were determined from the plot [**1**] versus k_{app}, (Figure 2B; Table 1). The K_d for the encounter complex = 2.27 μM, which is approximately 6000-fold higher than that measured at equilibrium. The second slow decrease in tryptophan emission is independent of [**1**], indicating a rate-limiting event, and probably represents the process leading to the formation of the high affinity complex observed at equilibrium.

The complex formed between sc11F8 and **1** is too tight for the dissociation to be measured by dilution and, therefore, was measured by displacement using **1**AP. This ligand, which has the same binding parameters as **1**, (Table 1), was bound to sc11F8 and then mixed rapidly (1:1) with an excess of **1**. By monitoring the fluorescence of **1**AP as it dissociates from sc11F8, the rate of dissociation can be measured directly and yields a value of 0.000 75 s^{-1} (Figure 2C). This rate is significantly slower than the value of k_{-1} estimated from Figure 2B (13.5 s^{-1}) and suggests that the dissociation of the complex is rate limited by the reversal of the second slow step of binding. On the basis of the relationship below, the K_d at equilibrium for the sc11F8·**1** complex can be estimated

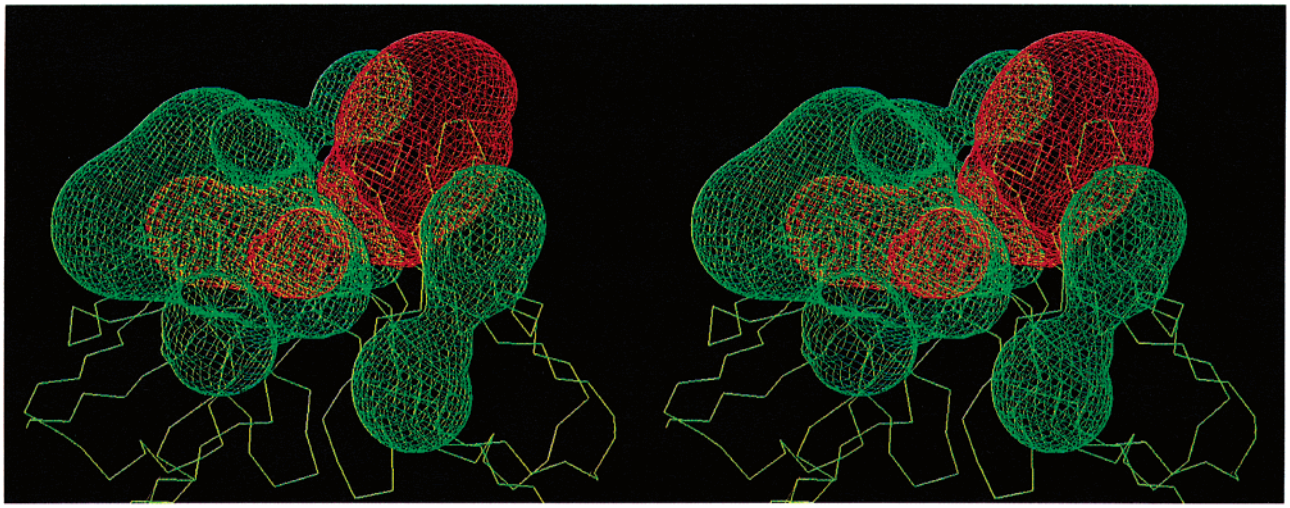

FIGURE 3: Electrostatic surface potential map of the CDR loops of 11F8. Areas of positive (green) and negative (red) electrostatic potential were calculated using the DELPHI module of the INSIGHT software (Biosym Technologies). Protein formal charges were assigned using preset DELPHI values for pH 7.4 (arginine = +1, lysine = +1, histidine = + 0.5, aspartate = −1, and glutamate = −1). The solute (*F*(ab)) dielectric constant was set to 2.0, while the solvent dielectric was set to 80 and the solvent ionic strength defined as 0.145 M. The result is displayed as a contour range map of two levels (±1).

$$K_{\text{d equilibrium}} = \frac{k_{-1} \cdot k_{-2}}{k_1 \cdot k_2} \qquad (3)$$

and gives a value of 0.29 nM, which is in good agreement with the K_d calculated from equilibrium measurements (0.31 ± 0.1 nM). Collectively, the data indicate that the binding mechanism described in Scheme 1 is sufficient to fit the data presented.

Binding of **1**AP by the parent 11F8 IgG results in a biphasic increase in the fluorescence of AP (*13*). The initial change in emission corresponds to the first binding step and the second slower increase represents the putative conformational change. On binding sc11F8, **1**AP only reports a single increase in fluorescence (Figure 2D). This change is slow (6 s^{-1}) and independent of [DNA], suggesting that the second binding step is being observed. Comparison of the kinetic parameters for the formation of 11F8 and sc11F8 complexes with **1** reveals small changes in each of the corresponding four rates. These data indicate that although the final affinities of the two complexes are the same, the rates at which the complexes are formed are slightly different. It is likely that the small variation in the kinetic binding parameters between the parent antibody and single-chain construct originates from additional flexibility between the variable domains that is usually imposed by the constant domains in the parent IgG or F(ab) (*16*−*18*).

Role of Binding Site Residues in Recognition. The kinetic basis of sequence-specific recognition by 11F8 is mediated principally through the dissociation of the complex. This conclusion was based upon a comparison of the kinetic binding parameters for the interaction between 11F8, **1**, a noncognate sequence, and a nonspecific sequence (*13*). Binding of the latter two ligands by 11F8 results in the formation of multiple encounter and final complexes due to overlapping binding sites present on the DNA (*8*, *13*).

Consequently, these sequences cannot be used to study the role of individual amino acids in the binding mechanism of sc11F8, as it does not necessarily follow that the role of the individual side chains is the same in the different complexes. Therefore, our studies focus exclusively on the interaction of sc11F8 with **1**.

The Role of Basic Residues in Binding. Assessing the effects of ionic strength on the rates of association, it was concluded that the initial association step between 11F8 and **1** is governed predominantly by electrostatic interactions (*13*). Electrostatic steering mediated by the negatively charged phosphate backbone and positively charged residues on 11F8 may increase the rate at which the two molecules approach each other before an initial encounter. This phenomenon has been proposed for other protein·nucleic acid and antibody−antigen complexes and is implied by an association rate that is higher than the modified Smolouchski limit for a diffusion-limited interaction (*19*−*22*). The CDR loops of sc11F8 contain seven basic side chains and electrostatic calculations suggest these give rise to a positively charged surface (Figure 3). Two of these amino acids, ^{R31}HCDR1 and ^{R98}HCDR3, form salt bridges with the phosphate backbone, and a third, ^{R96}HCDR3, is required for the structural integrity of the protein (*14*). The remaining four basic residues in the CDR loops were targeted for mutagenesis. ^{K62}HCDR2, ^{K64}HCDR2, ^{R24}LCDR1, and ^{K52}LCDR2 were each replaced with a glutamine, and an additional mutant was constructed where all four residues were substituted with glutamine (Quad). If these residues are involved in guiding ssDNA ligands to the binding site on sc11F8, their absence should cause a decrease in k_1, but have only a small effect on the overall stability of the complex.

Equilibrium binding experiments show that replacing any of these basic residues does not affect the number of cations released (data not shown), and the only difference in affinity is a 2-fold decrease for the Quad·**1** complex ($\Delta\Delta G$ = 0.40 kcal/mol relative to wild-type; Table 2). Small decreases in k_1 are observed for each of the individual mutants; however, when all four are removed, only a single decrease in tryptophan emission is observed upon mixing. The rate of the signal change is independent of [**1**] and thus represents the second slow binding step. These data indicate that the effect of the individual mutations is small, and subtle changes in the subsequent binding step can compensate for the small

Table 2: Kinetic Parameters for the Association and Dissociation of the sc11F8 and Arginine Mutants

complex	k_1 (μM^{-1} s^{-1})	k_{-1} (s^{-1})	k_2 (s^{-1})	k_{-2} (s^{-1})[a]	K_d (nM)
sc11F8·**1**	5.93 ± 0.64	13.5 ± 1.4	6.43 ± 0.34	0.00075 ± 0.00006	0.31 ± 0.1
$R24_LQ$·**1**	4.70 ± 0.23	13.3 ± 1.0	5.81 ± 0.51	0.00072 ± 0.00006	0.22 ± 0.1
$K52_LQ$·**1**	5.32 ± 0.57	12.9 ± 1.5	6.12 ± 0.70	0.00084 ± 0.00005	0.33 ± 0.2
$K62_HQ$·**1**	5.21 ± 0.49	12.4 ± 1.8	6.29 ± 0.55	0.00064 ± 0.00006	0.31 ± 0.1
$K64_HQ$·**1**	4.96 ± 0.37	13.0 ± 0.9	5.77 ± 0.63	0.00082 ± 0.00007	0.27 ± 0.1
Quad·**1**	−	−	6.68 ± 0.22	0.00086 ± 0.00007	0.65 ± 0.2
R98K·**1**	5.64 ± 0.65	13.0 ± 1.4	6.36 ± 0.26	0.00081 ± 0.00006	0.32 ± 0.2
R98Q·**1**	−	−	3.28 ± 0.40	0.0026 ± 0003	1.6 ± 0.4
R31K·**1**	7.56 ± 0.23	16.9 ± 1.2	3.55 ± 0.35	0.0022 ± 0002	3.4 ± 0.4
R31Q·**1**	−	−	2.79 ± 0.41	0.0045 ± 0.0003	9.3 ± 1.7

[a] Determined using the **1**AP sequence as described in Materials and Methods.

loss in affinity of the encounter complex due to the decrease in k_1. The effect of the mutagenesis on k_1 for the Quad·**1** complex cannot be determined experimentally so the contribution (if any) of these four basic side chains to electrostatic steering cannot be fully determined. However, it is apparent that collectively, the four basic residues are important for the conformation of the encounter complex.

Mutagenesis studies designed to investigate the role of basic residues in electrostatic steering in other protein−ligand systems have primarily targeted residues that are involved in known ionic contacts. In these studies, replacing a basic residue decreases both k_{on} and the binding affinity, but these experiments reflect the absence of the ionic contacts as well as changes in the electrostatic potential between the two binding interfaces. However, the negligible effect on the affinity of the Quad·**1** complex by these lysine/arginine mutants is consistent with that observed in protein−protein interactions (*23*, *24*), including the thrombin·hirudin complex, where the charged residues are thought to guide the two molecules together but are not involved in specific ionic contacts (*25*).

The dependence of k_1 and k_{-1} on salt concentration for the interaction between 11F8 and **1** indicate that the ionic contacts made between ^{R98}HCDR3 and ^{R31}HCDR1 and the phosphate backbone of **1** form during the first step (*13*, *14*). In addition to forming a salt bridge, R31 also makes base specific contacts (presumably hydrogen bonds) with dG_7−dC_{12} that are critical for sequence-specific binding (*14*). By replacing ^{R31}HCDR1 with lysine, the ionic contact can be preserved but the ability to form specific contacts through the guanidinium group is eliminated. As ^{R31}HCDR1 is already involved in the formation of the encounter complex via a salt bridge, it is possible that base specific contacts also form during the initial binding step. By comparing the rate constants of sc11F8 and R31K binding to **1**, the step in which sequence-specific contacts are made can be determined. First, to correct for possible variations in association due to the arginine to lysine exchange, the kinetics of R98K binding to **1** were investigated. Mutagenesis data indicate that ^{R98}HCDR3 is only involved in salt bridge formation, thus substitution with lysine should result in similar kinetic parameters to sc11F8 on binding to **1**. The kinetic parameters for R98K·**1** show little difference to those measured for the sc11F8·**1** complex, which suggests that substitution with lysine has little effect on the binding parameters (Table 2). The data for R31K binding to **1** reveals that k_1 is decreased and k_{-1} is increased compared to sc11F8, suggesting that the interaction between dG_7−dC_{12} and ^{R31}HCDR3 occurs during step one. Therefore, it is likely that the loss of affinity and specificity for **1** relative to wild-type by R31K originates in the first binding step.

Interruption of the ionic contacts formed between ^{R31}HCDR1 and ^{R98}HCDR3 and the phosphate backbone should predominantly effect step one through a decrease in k_1 and an increase in k_{-1}. Binding of **1** by either R31Q or R98Q results in a single decrease in tryptophan fluorescence, the rates of which are slow (∼3 s^{-1}) and independent of [**1**] and thus represent the second binding step (Table 2). These findings indicate that the loss of either salt bridge results in an altered conformation of the encounter complex. The values of k_2 for both the R31Q·**1** and R98Q·**1** complexes are significantly slower than that measured for sc11F8·**1** (Table 2). The change in k_2 could result from differences in the final conformation of the complexes or from the higher energy barrier that the encounter complexes would have to surmount to reach the same bound geometry. Footprinting experiments that compare the degree and pattern of protection of elements within the recognition epitope of **1** reveal no large structural differences between the sc11F8·**1** and R98Q·**1** complexes (*14*). However, significant differences are observed in the footprint of the R31Q·**1** complex relative to wild-type (*14*). Therefore, it is probable that the effect of the salt bridge made by R98 is small and the interactions that occur during step two in the R98Q·**1** complex can compensate for the absence of the ionic contact. Thus, the reduction in k_2 is representative of the higher energetic barrier that results from this process. For R31Q·**1**, a larger change in the encounter complex is predicted, presumably due to the absence of base specific contacts. This change cannot be compensated for during step two and results in a different final complex.

In summary, a combination of the positively charged side chains within the antigen binding site of 11F8 attract the negatively charged DNA ligand, thereby increasing the rate at which the DNA and protein initially associate. The ensuing encounter complex is then stabilized by the formation of two salt bridges between ^{R31}HCDR1 and ^{R98}HCDR3 and the phosphate backbone as well as base specific contacts formed between ^{R31}HCDR1 and dG_7−dC_{12}. Ultimately, only the interruption of the base specific contacts formed via ^{R31}HCDR1 affects the conformation of the final complex.

Role of the Hydrophobic Side Chains. The predominant driving force for the interaction of 11F8 with **1** arises from the release of water molecules from hydrophobic surfaces at the binding interface (*12*). Equilibrium binding studies show that four residues have an effect on desolvation: ^{W33}HCDR1, ^{L97}HCDR3, ^{Y100}HCDR3, and ^{Y32}LCDR1 (*14*).

Table 3: Kinetic Parameters for the Association and Dissociation of the Interaction between the Hydrophobic Mutations of sc11F8 and **1** or **1**AP

complex	k_1 (μM^{-1} s^{-1})[a]	k_{-1} (s^{-1})[a]	k_2 (s^{-1})	k_{-2} (s^{-1})	K_d (nM)[a]
sc11F8·**1**AP	5.93 ± 0.64	13.5 ± 1.4	6.43 ± 0.34	0.00075 ± 0.00006	0.31 ± 0.1
W33F·**1**AP	−	−	3.25 ± 0.24	0.001 ± 0.0002	0.45 ± 0.1
W33V·**1**AP	−	−	2.54 ± 0.31	0.0032 ± 0.0001	1.11 ± 0.3
L97A·**1**AP	−	−	3.01 ± 0.12	0.0019 ± 0.0009	0.64 ± 0.1
Y100F·**1**AP	5.89 ± 0.49	13.3 ± 1.1	5.57 ± 0.58	0.00085 ± 0.00001	0.334 ± 0.1
Yl00V·**1**AP	−	−	3.58 ± 0.30	0.0095 ± 00043	1.66 ± 0.3
$Y32_LF$·**1**AP	6.12 ± 0.53	12.7 ± 1.2	6.53 ± 0.15	0.00062 ± 0.00005	0.25 ± 0.1
$Y32_LA$·**1**AP	−	−	3.97 ± 0.36	0.00248 ± 0.00001	0.76 ± 0.2

[a] Measured using changes in tryptophan emission as described in Materials and Methods.

Aromatic residues often play a role in protein·nucleic acid complexes, including anti-DNA·DNA, through base stacking and/or hydrogen bonding, as observed in the DNA-1·dT_5 and BV04−01·$d(pT)_3$ complexes (*26*, *27*). Stacking as the source of desolvation for 11F8 binding to **1** is supported by footprinting and affinity data for the ^{Y32}LCDR1, ^{Y100}HCDR3, and ^{W33}HCDR1 alanine and valine substitutions (*14*).

Previous studies measuring the dependence of k_2 and k_{-2} on bulk solution polarity for the 11F8·**1** complex reveals that desolvation occurs during the second binding step. Therefore, mutations of the hydrophobic side chains should predominantly effect this step and have little effect in the formation of the encounter complex. Since the affinity of $Y32_LF$ and Y100F for **1** is similar to sc11F8, the kinetic parameters for the association and dissociation should also be similar to the wild-type protein. As shown in Table 3, the kinetic parameters for the phenylalanine mutants of ^{Y32}LCDR1 and ^{Y100}HCDR3 show little difference to those observed for sc11F8. When ^{W33}HCDR1 is replaced with a phenylalanine, only a single change in tryptophan fluorescence corresponding to the second binding step is detected. A decrease in affinity of the final complex is also observed, and these findings suggest a role for the tryptophan in the formation of the encounter complex. Binding of all the mutants that have a decrease in affinity for **1** at equilibrium only exhibit a single change in fluorescence emission. The rate of this signal change is slow and independent of [**1**] and therefore is describing the second binding step.

The sensitivity of the tryptophan fluorescence to the formation of the encounter complex infers a role of these hydrophobic residues in the initial binding step. However, these data do not agree with the preequilibrium results, indicating that electrostatic interactions are the dominant driving force during step one. Alternatively, it is possible that the signal change associated with k_1 originates from ^{W33}HCDR1. This residue lies centrally within the proposed binding pocket and would be susceptible to small changes in its environment as the DNA approaches the binding site. This hypothesis is consistent with the absence of a fast signal change for the formation of the W33F·**1** complex, where no significant change in the first step would be predicted compared to the wild type. In this complex, only a small increase in K_d (1.5-fold) is measured at equilibrium. The remaining signal change observed upon binding must arise from a combination of the four other tryptophan residues found in the framework region of the variable domains. Three of these residues immediately proceed a CDR loop, including HCDR3, which is known to be important for binding (*14*). Consequently, these tryptophan residues would be more sensitive to change in loop conformation that might occur in step two of the interaction, rather than the formation of the initial encounter complex.

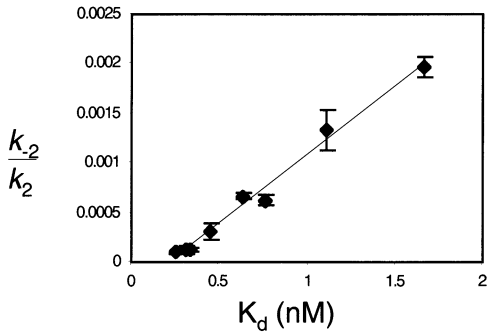

FIGURE 4: Relationship between k_{-2}/k_2 and K_d. This linear relationship indicates that the effect of the hydrophobic mutations on the affinity of the complex is mediated almost entirely through the second binding step.

There is a small (0.6−2.5-fold) difference in k_2 for each of the W33F, W33V, L97A, Y100F, Y100V, $Y32_LF$, and $Y32_LA$ complexes with **1** compared to wild-type, but up to a 12-fold difference in the rates of dissociation. Since k_{-2}/k_2 reflects the differences in affinity measured at equilibrium (Figure 4), the affinity of the final complexes is mediated through the second step of the interaction predominantly through the dissociation of the final complex. These findings suggest that the side chains of these residues have a minimal effect on the formation of the encounter complex, despite the loss of tryptophan signal, and thus support the hypothesis discussed above.

For 11F8 and sc11F8, the kinetic basis for sequence-specific recognition for **1** is mediated predominantly through changes in k_{-2} (*13*). Similarly, the specificity of many other protein·nucleic acid and antibody−antigen complexes is modulated through the rate of dissociation (*28*−*31*). Equilibrium binding experiments of ^{Y32}LCDR1, ^{W33}HCDR1, ^{L97}HCDR3, and ^{Y100}HCDR3 indicate that only the replacement of ^{Y100}HCDR3 decreased specificity for **1**, although the other three residues are involved in binding (*14*). The kinetic data shows that the formation of the ^{Y100}V·**1** complex is 1.6-fold slower than that for the sc11F8·**1**, but it dissociates 12-fold more quickly, indicating that specific interactions associated with ^{Y100}HCDR3 are mediated through the dissociation of the final complex.

Temperature Dependence of Binding. Binding of sc11F8 to **1** is enthalpically favorable, entropically unfavorable, and accompanied by a negative change in heat capacity (*12*). These thermodynamic parameters arise from the desolvation of the hydrophobic binding interfaces that become buried

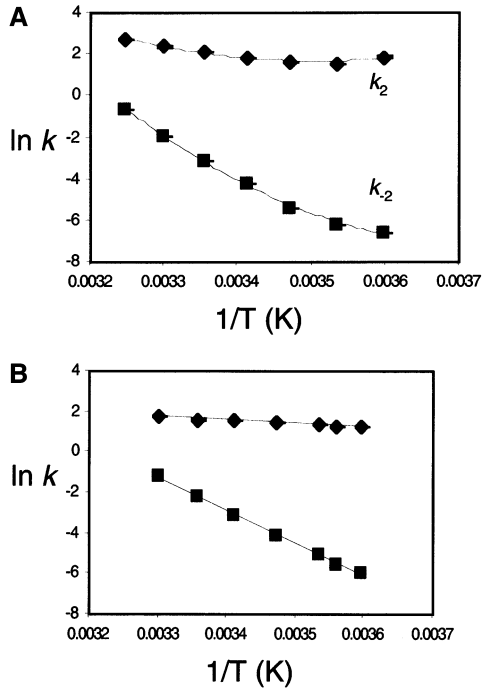

FIGURE 5: Arrhenius plots for the second step of the interaction for (A) sc11F8·**1** and (B) Y100V·**1**. In both plots, ◆ represents the effect of temperature on k_2 and ■ on k_{-2}. The error associated with each value is <5%. Curvature is observed for the results of the sc11F8·**1** complex probably reflecting the change in heat capacity on the formation of this complex observed at equilibrium (*14*). No such curvature is observed for the formation of the Y100V·**1** complex. The activation energy for each step is calculated from the slope of these plots as described in Materials and Methods and given in Table 4.

Table 4: Thermodynamic Parameters for the Second Binding Step[a]

complex	k_2 (kcal/mol)	k_{-2} (kcal/mol)
	Part A	
sc11F8·**1**AP	9.51 ± 0.52	34.6 ± 1.5
W33F·**1**AP	7.58 ± 0.31	29.0 ± 2.3
W33V·**1**AP	4.98 ± 0.22	26.3 ± 1.8
L97A·**1**AP	5.57 ± 0.36	33.9 ± 2.1
Y100F·**1**AP	7.62 ± 0.21	38.6 ± 1.8
Y100V·**1**AP	3.19 ± 0.16	20.9 ± 0.9
$Y32F_L$·**1**AP	9.42 ± 0.32	35.2 ± 3.0
$Y32A_L$·**1**AP	6.10 ± 0.47	31.8 ± 1.7
	Part B	
sc11F8·**1**AP	8.47 ± 0.41	32.5 ± 2.3
W33F·**1**AP	7.03 ± 0.35	27.7 ± 1.4
W33V·**1**AP	4.56 ± 0.32	24.7 ± 1.2
L97A·**1**AP	4.99 ± 0.17	31.3 ± 2.7
Y100F·**1**AP	7.32 ± 0.26	36.1 ± 2.1
Y100V·**1**AP	2.59 ± 0.17	19.7 ± 2.5
$Y32_LF$·**1**AP	7.83 ± 0.43	33.2 ± 2.1
$Y32_LA$·**1**AP	5.34 ± 0.31	30.8 ± 1.8
	Part C	
sc11F8·**1**AP	−25.1 ± 1.3	50.9 ± 4.2
W33F·**1**AP	−29.9 ± 3.6	56.9 ± 2.1
W33V·**1**AP	−39.4 ± 4.9	45.6 ± 3.5
L97A·**1**AP	−28.4 ± 2.5	49.1 ± 3.2
Y100F·**1**AP	−29.3 ± 3.5	62.2 ± 4.3
Y100V·**1**AP	−46.6 ± 4.1	43.7 ± 3.7
$Y32_LF$·**1**AP	−26.7 ± 1.7	68.6 ± 4.6
$Y32_LA$·**1**AP	−31.5 ± 2.4	39.5 ± 3.8

[a] Part A: activation energies for the association and dissociation of the second step of the interactions between the different hydrophobic mutants of Sc11F8 and **1**AP. Part B: the enthalpies of activation for the second step calculated from the Eyring equation. Part C: the entropies of activation calculated from the *y*-intercept of the Eyring plot, given at 25 °C.

on complexation. To determine whether the equilibrium thermodynamic parameters arise predominantly from the processes that occur during the second binding step as suggested by the data in Table 3, the interaction between sc11F8 and hydrophobic mutants with **1** were measured over the temperature range of 5−35 °C. As the initial binding step is impossible to detect in its entirety at higher temperatures using tryptophan fluorescence, the **1**AP sequence was used since it does not detect step one.

The Arrhenius plot for k_2 and k_{-2} of sc11F8·**1** is shown in Figure 5A. There is some curvature in the plot, particularly in temperatures below 20 °C. Nonlinear Arrhenius plots are often interpreted as the results of two or more processes occurring simultaneously that have different temperature coefficients (*32*). However, they have also been observed for interactions that are accompanied by a change in heat capacity (*32*−*34*). Curvature is observed for each of the complexes that exhibit a change in heat capacity at equilibrium (sc11F8·**1**, Y100F·**1**, and $Y32_LF$·**l**), while the plots are linear for those complexes that do not (W33F·**1**, W33V·**1**, L97A·**1** Y100V−**l** and $Y32_LA$·**1**; Figure 5B). These findings indicate that the change in heat capacity is causing the nonlinear Arrhenius plots and that it associated with hydrophobic interactions occurring in the second binding step.

The activation energies (E_a) for the k_2 and k_{-2} steps are given in Table 4. For those complexes exhibiting curvature, E_a was calculated at 25 °C. The magnitude of E_a for the dissociation of the complexes reflects the differences in affinity for **1** by the mutant proteins. In each complex, the enthalpy of activation ($\Delta H^{\ddagger}$) is positive as expected from the energy required for the making and breaking of bonds during the association and dissociation processes. The size of $\Delta H^{\ddagger}$ for both the association and dissociation step emulate the affinity of the complex at equilibrium; i.e., the smaller the value of $\Delta H^{\ddagger}$, the lower the affinity of the complex. The entropy of activation ($\Delta S^{\ddagger}$) for k_2 is usually predicted to be zero or slightly positive as the isomerization step is a unimolecular event (*35*). Consequently most of the rotational, vibrational and translational freedom of the interacting molecules has already been lost and water release from the interacting surfaces would give a favorable entropy term (*32*). However, the release of water into bulk solution where all hydrogen bonding groups can be satisfied would give rise to the negative $\Delta S^{\ddagger}$ observed. The values of $\Delta S^{\ddagger}$ are small and sufficiently close in value that no analysis can be made regarding the effect of the individual mutations although there is a general decrease in $\Delta S^{\ddagger}$ as the affinities of the complex decrease. As would be expected, $\Delta S^{\ddagger}$ for k_{-2} is positive, representing the gain in freedom achieved by the two dissociating molecules and resolvation of the binding interfaces. The curvature exhibited in the Arrhenius plots and the negative values obtained for $\Delta S^{\ddagger}$ support the hypothesis that the thermodynamic parameters measured at equilibrium predominantly originate from processes that occur during the second binding step.

DISCUSSION

Prior studies have demonstrated that ^{Y32}LCDR1, ^{R31}HCDR1, ^{W33}HCDR1, ^{L97}HCDR3, ^{R98}HCDR3, and ^{Y100}HCDR3 within the CDR loops of sc11F8 account for approximately 80%

Scheme 2

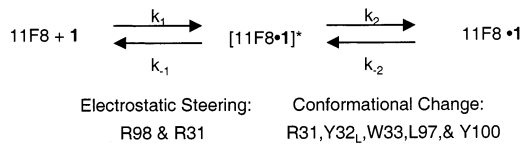

of the binding energy in the complex with **1**. ^{R31}HCDR1 and ^{Y100}HCDR3 alone account for 40% of the binding energy, and these two residues are critical for specific recognition of **1** (*14*). Our experiments reveal that sequence-specific recognition of **1** by 11F8 is mediated through interactions that occur in both binding steps. A model summarizing the proposed role of individual side chains is presented in Scheme 2. ^{R31}HCDR1, a somatic mutation that originates from a germline encoded serine residue, interacts with dG_7-dC_{l2}, positioning **1** in the correct orientation within the antigen binding site. This interaction apparently creates the optimum binding interface between ^{Y100}HCDR3 and T_{10} and T_{11} on **1**. The loss of the guadinium group of ^{R31}HCDR1 or the substitution of ^{Y100}HCDR3 with valine results in a loss of specificity that can be observed through an increase in k_{-2}.

The first step of binding, which is dominated by electrostatic interactions, also includes sequence-specific recognition of dG_7-dC_{12}. In diffusion-controlled protein·nucleic acid interactions, the first binding step is usually a nonspecific process, driven by long range electrostatic attraction between the interacting molecules. For example, EcoRI binds nonspecifically to dsDNA via electrostatic interactions and then "slides" along the helix until its specific binding sequence is found (*36*). Similarly, uracil DNA glycosylase binds non specifically to DNA until it locates a misplaced uracil when binding causes a conformational change within the DNA resulting in the flipping out of the uracil base. The uracil then stacks between aromatic residues of the protein (*37*). Initial nonspecific complexes have also been observed in protein·RNA systems. For example, the interaction between HIV-1 Tat peptide with TAR RNA is a diffusion controlled interaction resulting in a tight, but nonspecific complex (*38*). Similarly, the first step in recognition of U1 RNA by the U1A protein is mediated by electrostatic interactions. Here, sequence-specific binding is thought to occur through the interaction of R52 with the stem-loop junction of the U1A RNA, similar to the way in which ^{R31}HCDR1 on 11F8 interacts with **1** (*22*, *39*). While it is not yet know if R52 on U1A makes sequence-specific contacts during the first step of binding, overall, the kinetic, thermodynamics, and certain structural aspects of U1A·RNA interactions bear many similarities to the 11F8·**1** complex.

On the basis of the crystal structures of DNA-l·oligoT and BV04−01·oligoT complexes, Tanner et al. proposed a ssDNA-antibody recognition module whereby ^{Y32}LCDR1 stacks above a base and a second aromatic residue from HCDR3 stacks below (*26*). In this motif, the majority of contacts are made to the DNA bases. This is thought to enable the antibody to distinguish between ds- and ssDNA and possibly contributes to sequence specificity. Similar types of interactions have been observed for anti-RNA Je1103 mAb complexed with poly(rI) (*40*) and the U1A RNA binding protein, where C5 stacks between F56 and Y13 of U1A (*41*, *42*). Mutagenesis studies have illustrated that F56 is important for the specific recognition of the stem-loop II RNA sequence by the U1A protein through a network of hydrogen bonds and van der Waals that rely on the complimentarity of the binding interfaces. In this system, stacking interactions occur during the second binding step and the differences in affinity for various mutations of F56 are manifested by changes in the rates of dissociation of the complex (*42*), as observed in the sc11F8·**1** complex. 11F8 may bind ssDNA in a similar manner incorporating T_{10} and T_{11} of the binding epitope between ^{Y32}LCDR1, ^{Y100}HCDR3, and ^{W33}HCDR1, with L97 lying at the back of the binding pocket (*14*). This model permits ^{Y100}HCDR3, located centrally within the binding interface, to contribute to both affinity and specificity through a myriad of interactions as proposed for F56 in the U1A·RNA complex.

The "induced fit" mechanism of binding observed for sc11F8·**1** has been observed for other many other protein·nucleic acid complexes (*22*, *37*, *38*, *43*−*45*). In many cases, conformational changes that occur upon binding are biologically relevant; e.g., the newly formed surfaces resulting from the conformational adjustments are required for subsequent steps with functional significance (*43*). 11F8 provokes kidney inflammation in vivo by first binding to ssDNA adherent to the glomerular basement membrane. Sequence-specific interactions involving ^{R31}HCDR1 lead to conformational adjustments stabilized by ^{Y100}HCDR3, ultimately resulting in a slow rate of dissociation. Thus, it is possible that 11F8 is pathogenic because it remains bound to glomerular DNA antigens for a longer period of time than nonpathogenic anti-DNA, thereby permitting initiation of an inflammatory response. In support of this hypothesis, we find that nonpathogenic mAbs that differ from 11F8 by fewer than five amino acids, dissociate from **1** much faster than 11F8 (unpublished observations, 2003).

In summary, our data show that sequence specificity is mediated through interactions that take place in both binding steps. Although 11F8 binds ssDNA, this system reflects many features that are exhibited by protein·RNA complexes. At present SLE is treated using broad acting lymphotoxic drugs. Although effective in many patients, treatment with agents is accompanied by a range of serious side effects. However, the information collected about 11F8 binding (*8*, *10*, *12*−*14*) may help to facilitate the rational design of anti-DNA antagonists for the treatment of lupus. For example, an inhibitor with a sufficiently fast k_1 and a slow dissociation rate should effectively compete with DNA for binding to 11F8. We are presently exploring this possibility along with investigating the relationships between k_{-2} and pathogenicity as a means to differentiate pathogenic anti-DNA from those that are benign.

REFERENCES

1. Eilat, D., and Anderson, W. F. (1994) *Mol. Immunol. 31*, 1377−1390.
2. Pisetsky, D. S. (2001) *Immunol. Res. 22*, 119−126.
3. Chmielewski, J., and Schultz, P. (1991) *Tetrahedron 47*, 2563−2572.
4. Mian, S. A. R., Bradwell, A. R., and Olson, A. J. (1991) *J. Mol. Biol. 217*, 133−151.
5. Tan, E. M. (1989) *Adv. Immunol. 44*, 93−151.
6. Waer, M. (1990) *Clin. Rheum. 9*, Suppl. 1, 111−114.
7. Isenberg, D. A., Ehrenstein, M. R., Longhurst, C., and Kalsi, J. K. (1994) *Arthritus Rheum. 37*, 169−180.

8. Swanson, P. C., Ackroyd, P. C., and Glick, G. D. (1996) *Biochemistry 35*, 1624−1633.
9. Swanson, P. C., Yung, R. L., Blatt, N. B., Eagan, M. A., Norris, J. M., Richardson, B. C., Johnson, K. J., and Glick, G. D. (1996) *J. Clin. Invest. 97*, 1748−1760.
10. Stevens, S. Y., and Glick, G. D. (1999) *Biochemistry 38*, 560−568.
11. Terada, K., Okuhara, E., Kawarada, Y., and Hirose, S. (1991) *Biochem. Biophys. Res. Commun. 174*, 323−330 and references therein.
12. Ackroyd, P. C., Cleary, J., and Glick, G. D. (2001) *Biochemistry 40*, 2911−2922.
13. Beckingham, J. A., and Glick, G. D. (2001) *Bioorg. Med. Chem. 9*, 2243−2252.
14. Cleary, J., and Glick, G. D. (2003) *Biochemistry, 42*, 30−41.
15. Blatt, N. B., Bill, R. M., and Glick, G. D. (1998) *Hybridoma 17*, 33−39.
16. Cupit, P. M., Lorenzen, N., Strachan, G., Kemp, G. J. L., Secombes, C. J., and Cunningham, C. (2001) *Virus Res. 81*, 47−56.
17. Mallender, W. D., Carrero, J., and Voss, E. W. J. (1996) *J. Biol. Chem. 271*, 5338−5346.
18. Worn, A., and Pluckthun, A. (2001) *J. Mol. Biol. 305*, 989−1010.
19. Kozack, R. E., M. J., d. M., and Subramaniam, S. (1995) *Biophys. J. 68*, 807−814.
20. Weidenhaupt, M., Khalif, M. B., Hugo, H., Choulier, L., Altschuh, D., and Vernet, T. (2002) *J. Mol. Recognit. 15*, 94−103.
21. Lago, H., Parrott, A. M., Moss, T., Stonehouse, N., and Stockley, P. G. (2001) *J. Mol. Biol. 305*, 1131−1144.
22. Katsamba, P. S., Myszka, D. G., and Laird-Offringa, I. A. (2001) *J. Biol. Chem. 276*, 21476−21481.
23. Selzer, T., and Schreiber, G. (1999) J. *Mol. Biol. 287*, 409−419.
24. Selzer, T., Albeck, S., and Schreiber, G. (2000) *Nat. Struct. Biol. 7*, 537−541.
25. Myles, T., Le Bonniec, B. F., Betz, A., and Stone, S. R. (2001) *Biochemistry 40*, 4972−4979.
26. Tanner, J. J., Komissarov, A. A., and Deutscher, S. L. (2001) *J. Mol. Biol. 314*, 807−822.
27. Herron, J. N., He, X. M., Ballard, D. W., P. R., B., Pace, P. E., Blothwell, A. L. M., Voss, E. W. J., and Edmundson, A. B. (1991) *Proteins 11*, 159−175.
28. Hart, D. J., Speight, R. E., Cooper, M. A., Sutherland, J. D., and Blackburn, J. M. (1999) *Nucleic Acids Res. 27*, 1063−1069.
29. Lavoie, T. B., Mohan, S., Lipschultz, C. A., Grivel, J.-C., Li, Y., Mainhart, C. R., Kam-Morgan, L. N. W., Drohan, W. N., and Smith-Gill, S. J. (1999) *Mol. Immunol. 36*, 1189−1205.
30. Seimiya, M., and Kurosawa, Y. (1996) *FEBS Lett. 398*, 279−284.
31. Malkov, V. A., and Camerini-Otero, R. D. (1998) *J. Mol. Biol. 278*, 317−330.
32. Gutfreund, H. (1995) *Kinetics for the Life Sciences*, Cambridge University Press, Cambridge.
33. Fedoriw, A. M., Liu, H., Anderson, V., and deHaseth, P. L. (1998) *Biochemistry 37*, 11971−11979.
34. Petri, V., Hsieh, M., Jamison, E., and Brenowitz, M. (1998) *Biochemistry 37*, 15842−15849.
35. Jencks, W. P. (1969) *Catalysis in Chemistry and Enzymology*, McGraw-Hill, New York.
36. Stanford, N. P., Szczelkun, M. D., Marko, J. F., and Halford, S. E. (2000) *EMBO J. 19*, 6546−6557.
37. Stivers, J. T., Pankiewicz, K. W., and Watanabe, K. A. (1999) *Biochemistry 38*, 952−963.
38. Metzger, A. U., Bayer, P., Willbold, D., Hoffmann, S., Frank, R. W., Goody, R. S., and Rosch, P. (1997) *Biochem. Biophys. Res. Commun. 241*, 31−36.
39. Tang, Y., and Nilsson, L. (1999) *Biophys. J. 77*, 1284−1305.
40. Pokkuluri, R. P., Bouthillier, F., Li, Y., Kuderova, A., Lee, J. C., and Cygler, M. (1994) *J. Mol. Biol. 243*, 283−297.
41. Allain, F. H.-T., Howe, P. W. A., Neuhaus, D., and Varani, G. (1997) *EMBO J. 16*, 5764−5772.
42. Shiels, J. C., Tuite, J. B., Nolan, S. J., and Baranger, A. M. (2002) *Nucleic Acids Res. 30*, 550−558.
43. Perez-Canadillas, J.-M., and Varani, G. (2001) *Curr. Opin. Struct. Biol. 11*, 53−58.
44. Parkhurst, K. M., Richards, R. M., Breowitz, M., and Parkhurst, L. J. (1999) J. *Mol. Biol. 289*, 1327−1341.
45. Sha, M., Wang, Y., Xiang, T., van Heerden, A., Browning, K. S., and Goss, D. J. (1995) *J. Biol. Chem. 270*, 29904−29909.

BI020658K